ELSEVIER

Earth and Planetary Science Letters 186 (2001) 15–31

EPSL

www.elsevier.com/locate/epsl

^{226}Ra–^{230}Th–^{238}U disequilibria of historical Kilauea lavas (1790–1982) and the dynamics of mantle melting within the Hawaiian plume

Aaron J. Pietruszka *, Kenneth H. Rubin, Michael O. Garcia

Hawaii Center for Volcanology, Department of Geology and Geophysics, University of Hawaii, Honolulu, HI 96822, USA

Received 13 January 2000; accepted 3 January 2001

Abstract

The geochemical variations of Kilauea's historical summit lavas (1790–1982) document a rapid fluctuation in the mantle source and melting history of this volcano. These lavas span nearly the entire known range of source composition for Kilauea in only 200 yr and record a factor of ~2 change in the degree of partial melting. In this study, we use high-precision measurements of the U-series isotope abundances of Kilauea's historical summit lavas and two 'ingrowth' models (dynamic and equilibrium percolation melting) to focus on the process of melt generation at this volcano. Our results show that the ^{226}Ra–^{230}Th–^{238}U disequilibria of these lavas have remained relatively small and constant with ~12 ± 4% excess ^{226}Ra and ~2.5 ± 1.6% excess ^{230}Th (both are ± 2σ). Model calculations based mostly on subtle variations in the ^{230}Th–^{238}U disequilibria suggest that lavas from the 19th to early 20th centuries formed at significantly higher rates of mantle melting and upwelling (up to a factor of ~10) compared to lavas from 1790 and the late 20th century. The shift to higher values for these parameters correlates with a short-term decrease in the size of the melting region sampled by the volcano, which is consistent with fluid dynamical models that predict an exponential increase in the upwelling rate (and, thus, the melting rate) towards the core of the Hawaiian plume. The Pb, Sr, and Nd isotope ratios of lavas derived from the smallest source volumes correspond to the 'Kilauea' end member of Hawaiian volcanoes, whereas lavas derived from the largest source volumes overlap isotopically with recent Loihi tholeiitic basalts. This behavior probably arises from the more effective blending of small-scale source heterogeneities as the melting region sampled by Kilauea increases in size. The source that was preferentially tapped during the early 20th century (when the melt fractions were lowest) is more chemically and isotopically depleted than the source of the early 19th and late 20th century lavas (which formed by the highest melt fractions). This inverse relationship between the magnitude of source depletion and melt fraction suggests that source fertility (i.e. lithology) controls the degree of partial melting at Kilauea. Thus, rapid changes in the size of the melting region sampled by the volcano (in the presence of these small-scale heterogeneities) may regulate most of the source- and melting-related geochemical variations observed at Kilauea over time scales of decades to centuries.

Keywords: Kilauea; volcanoes; Hawaii; lavas; geochemistry; uranium; isotopes; mantle plumes; melting; models

* Corresponding author. Present address: Carnegie Institution of Washington, Department of Terrestrial Magnetism, 5241 Broad Branch Road, N.W., Washington, DC 20015, USA. Tel.: +1-202-478-8476; E-mail: pietrus@dtm.ciw.edu

0012-821X/01/$ – see front matter
PII: S0012-821X(01)00230-8

1. Introduction

Historical lavas from active Hawaiian shield volcanoes such as Kilauea and Mauna Loa are ideal for investigating mantle melting because they display systematic melting-related variations of incompatible trace element ratios (e.g. La/Yb or Nb/Y) over short periods of time (years to decades [1–4]). Models based on these fluctuations in lava chemistry suggest that the degree of partial melting has varied by a factor of ~2 for Kilauea since 1790 [3] and ~40% relative for Mauna Loa since 1843 [2], which are significant portions of the overall range inferred for Hawaiian shield volcanoes (a factor of ~2.5 [5]). The origin of these short-term changes in the degree of partial melting is poorly understood, but may be related to the interplay between mantle melting and small-scale source heterogeneities [2,3]. A similar pattern of rapid, source- and melting-related geochemical variations has also been observed in stratigraphic sections of prehistorical shield lavas from Hawaiian volcanoes (e.g. Mauna Loa [6] and Mauna Kea [7,8]). Thus, a detailed geochemical sampling of lavas over time scales of decades to centuries may provide the best clues to understanding the dynamics of mantle melting within the Hawaiian plume.

The U-series isotope abundances of lavas (e.g. ^{230}Th and ^{226}Ra) are excellent tracers of mantle melting because the half-lives of ^{230}Th and ^{226}Ra (~75 kyr and 1600 yr, respectively) are thought to be similar to the time scale of magmatic processes (e.g. [9]). This unique feature of U-series isotopes offers the potential to study both the nature and timing of the processes that fractionate incompatible trace elements during magma genesis. This possibility derives from two important properties of the ^{238}U decay chain. First, prior to melting, the source regions of basaltic lavas will generally be in a state of radioactive, or secular, equilibrium in which the ^{238}U, ^{230}Th, and ^{226}Ra activities (decay rates) are equal. When secular equilibrium prevails, the (^{230}Th/^{238}U) and (^{226}Ra/^{230}Th) ratios (parentheses indicate activities) of the source are known (and equal to unity), in contrast to most other geochemical tracers of the melting process (e.g. stable, incompatible trace elements). Second, any process that fractionates these elements, such as partial melting of the mantle, induces a state of radioactive disequilibrium in which the activities of ^{238}U,

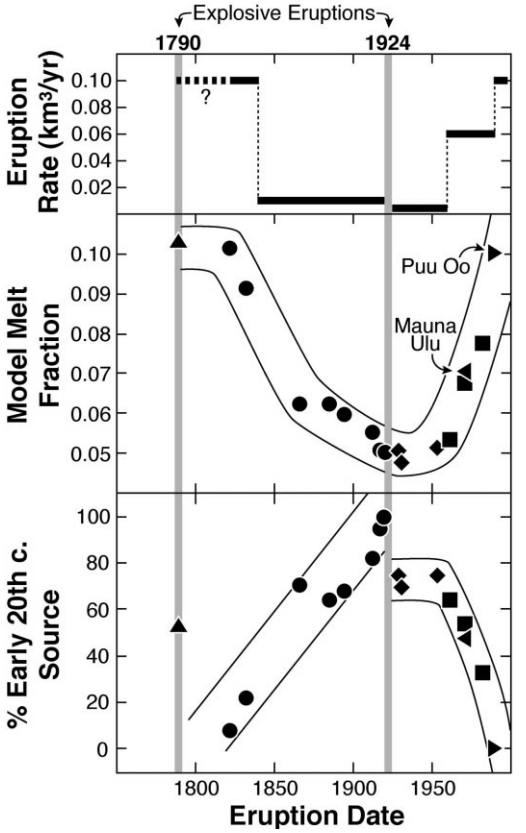

Fig. 1. Summary of the melting, source, and eruptive history of Kilauea Volcano. Kilauea's historical lavas record a rapid fluctuation in the degree of partial melting (inferred from incompatible trace elements) that correlates with the volcano's eruption rate (and, presumably, its magma supply rate). The composition of the mantle source region tapped by Kilauea (or proportions of the source components) has also changed over time (shown as a % of the early 20th century source composition, which corresponds to the 'Kilauea' isotopic end member for Hawaiian volcanoes). The vertical shaded lines mark the explosive summit eruptions of 1790 and 1924. See [3] for the methods and/or references used to calculate each of these parameters. The average melt fraction and source composition for the Mauna Ulu rift zone lavas are estimated using data from [1] and unpublished Pb isotope analyses (A. Hofmann, personal communication, 1999). The sample symbols are grouped according to eruption date: up triangles (1790), circles (1820–1921), diamonds (1929–1954), squares (1961–1982), left triangles (Mauna Ulu), and right triangles (Puu Oo).

Table 1
Th, U, Ba, Sr and ^{226}Ra abundances, U-series isotope activity ratios, and Sr isotope ratios for the historical summit lavas of Kilauea Volcano

Sample	Eruption date	[Th] (μg g^{-1})	[U] (μg g^{-1})	[Ba] (μg g^{-1})	[Sr] (μg g^{-1})	[^{226}Ra] (fg g^{-1})	($^{230}Th/^{232}Th$)	($^{230}Th/^{238}U$)	($^{226}Ra/^{230}Th$)$_0$	($^{234}U/^{238}U$)	$^{87}Sr/^{86}Sr$
1790-1	1790	0.6960	0.2344	79.67	278.6	92.0 ± 0.7	1.049 ± 0.011	1.022	1.147	1.003 ± 0.004	0.703612
						91.4 ± 0.6	1.040 ± 0.011				
1820-1	1820–1823	0.7812	0.2641	98.34	310.6	98.6 ± 0.6	1.041 ± 0.015	1.014	1.103	1.003 ± 0.003	0.703638
						99.4 ± 0.8	1.039 ± 0.011				
1866	1866	1.156	0.3969	141.7	382.4						0.703548
1894-2 (groundmass)	1894	1.133	0.3931	144.2	385.1	162.7 ± 1.0	1.067 ± 0.016	1.020	1.212	1.004 ± 0.004	0.703547
							1.082 ± 0.009				
1894-2 (glass)	1894	1.201	0.4135	146.0	382.6						0.703548
95-TAJ-3	1912	1.254	0.4399	144.3	398.2						0.703536
1917	1917	1.206	0.4243	132.5	397.7	162.8 ± 1.8	1.093 ± 0.012	1.024	1.114	1.013 ± 0.003	0.703491
Kil1919	1919	1.225	0.4279	135.0	401.5	167.4 ± 1.3	1.085 ± 0.011	1.023	1.129	1.003 ± 0.002	0.703471
						165.0 ± 0.8					
1929	1929	1.306	0.4289	146.5	392.5	171.3 ± 2.5	1.035 ± 0.010	1.042	1.131	1.005 ± 0.003	0.703551
						168.7 ± 3.3	1.042 ± 0.013				
1931HM	1931–1932	1.336	0.4393	150.1	400.0						0.703546
1954-2	1954	1.287	0.4284	150.4	400.9						0.703607
K61-22	1961	1.232	0.4141	145.8	388.7	155.3 ± 1.1	1.048 ± 0.009	1.029	1.081	1.006 ± 0.003	0.703584
							1.051 ± 0.015				
1971S	Sep 1971	1.087	0.3633	132.0	386.4						0.703580
1982A-20	Apr 1982	0.9832	0.3297	121.3	360.1	126.2 ± 0.7	1.052 ± 0.014	1.029	1.103		0.703566
							1.042 ± 0.009				

All uncertainties are ±2σ. The reproducibility of the Th, U, Ba, and Sr concentrations (and ratios thereof) is ±0.3% or better. The uncertainties for the ^{226}Ra concentrations and the ($^{230}Th/^{232}Th$) and ($^{234}U/^{238}U$) ratios listed in the table are the within-run measurement errors. The ($^{230}Th/^{238}U$) and the age-corrected ($^{226}Ra/^{230}Th$) ratios are calculated using the average ^{226}Ra abundances and ($^{230}Th/^{232}Th$) ratios for each sample. The accuracy and reproducibility of our Th isotope ratio measurements were verified with the University of California Santa Cruz (UCSC) Th standard 'A'. Our average for UCSC Th 'A' was ($^{230}Th/^{232}Th$) = 1.086 ± 0.012 (n = 39), which is 0.3% lower than the predicted value (1.089). Replicate analyses of the National Institute of Science and Technology (NIST) U standard SRM U010 gave ($^{234}U/^{238}U$) = 0.9993 ± 0.0054 (n = 10), which is 0.04% higher than the certificate value (0.9989). Replicate analyses of the NIST Sr standard SRM 987 during two periods of time separated by a major machine upgrade gave $^{87}Sr/^{86}Sr$ = 0.710259 ± 0.000012 (n = 10) and $^{87}Sr/^{86}Sr$ = 0.710268 ± 0.000014 (n = 14). All data are expressed relative to $^{87}Sr/^{86}Sr$ = 0.710259 for SRM 987. The within-run uncertainties on individual $^{87}Sr/^{86}Sr$ measurements were always equal to or less than the external reproducibility of SRM 987. The total procedural blanks for abundance measurements were: Th (1–6 pg), U (2–7 pg), Ba (0.2–1 ng), Sr (20–60 pg), and ^{226}Ra (< 0.01 fg). Blank corrections of 0.003–0.04% for Th, 0.02–0.1% for U, and 0.005–0.07% for Ba were made to derive the final concentrations (Sr and ^{226}Ra blanks were negligible). The total procedural blanks for isotope ratio measurements were negligible: Th (10–20 pg) and U (3–4 pg). The decay constants used are: $\lambda^{238}U$ (1.551×10^{-10} yr^{-1}), $\lambda^{234}U$ (2.835×10^{-6} yr^{-1}), $\lambda^{232}Th$ (4.948×10^{-11} yr^{-1}), $\lambda^{230}Th$ (9.195×10^{-6} yr^{-1}), and $\lambda^{226}Ra$ (4.332×10^{-4} yr^{-1}).

^{230}Th, and ^{226}Ra are unequal. The magnitude of the ^{226}Ra–^{230}Th–^{238}U disequilibria in basaltic lavas is believed to depend, in part, upon the rates of mantle melting and upwelling [10–12].

Early U-series studies of Hawaiian shield lavas used radioactive decay counting techniques to identify small, but significant, ^{230}Th and ^{226}Ra excesses relative to their respective parents, ^{238}U and ^{230}Th, and proposed a magmatic (mantle melting) origin for these disequilibria [13–15]. More recent, high-precision decay counting and mass spectrometric U-series investigations of historical Kilauea and Mauna Loa lavas observed small ^{230}Th excesses and moderate ^{226}Ra excesses up to 28% [16–20]. Modeling of the small ^{226}Ra–^{230}Th–^{238}U disequilibria of these lavas (compared to mid-ocean ridge basalts [21,22] and lavas from other ocean island volcanoes [23]) has led to the idea that the rates of mantle melting and upwelling for tholeiitic basalt production within the Hawaiian plume are relatively high [16–19,23].

This paper presents new U-series isotope, Sr isotope, and trace element abundance data for the historical summit lavas of Kilauea Volcano (1790–1982). These samples span nearly the entire known range of source composition for this volcano and record a factor of $\sim$2 change in the degree of partial melting [3]. In this study, we focus on mantle melting at Kilauea using the U-series isotope systematics of its historical lavas and two 'ingrowth' models for producing ^{226}Ra–^{230}Th–^{238}U disequilibria (dynamic melting [10] and equilibrium percolation melting [12]). Our goal is to find an internally consistent model that accounts for the ^{226}Ra–^{230}Th–^{238}U disequilibria of Kilauea lavas in the context of other geochemical evidence (from incompatible trace elements and Pb, Sr, and Nd isotope ratios [3]) for a short-term change in the mantle source and melting history of this volcano (Fig. 1).

2. Results

High-precision measurements of the Ba, Th, U, Sr, and ^{226}Ra concentrations and (^{230}Th/^{232}Th), (^{230}Th/^{238}U), (^{226}Ra/^{230}Th), (^{234}U/^{238}U), and ^{87}Sr/^{86}Sr ratios of Kilauea's historical summit lavas by thermal ionization mass spectrometry (TIMS) are reported in Table 1 (for additional sample information and analytical methods see the **EPSL Online Background Dataset**[1]). In this section, we describe the temporal geochemical variations of the lavas (Fig. 2). All uncertainties are $\pm 2\sigma$.

2.1. ^{230}Th–^{238}U disequilibria

The ^{230}Th–^{238}U disequilibria of Kilauea lavas have remained nearly constant since 1790 ($\sim 2.5 \pm 1.6\%$, 2σ) with a narrow 1.4–4.2% range in the amount of excess ^{230}Th (Fig. 2). The ^{230}Th–^{238}U disequilibria from other recent studies of Kilauea lavas (except [19,20]) are significantly more variable than our results and include some samples with (^{230}Th/^{238}U) < 1 [16,17]. Despite the small (^{230}Th/^{238}U) range observed in this study, the samples display a systematic temporal variation. The (^{230}Th/^{238}U) ratios increase subtly from the 19th to early 20th centuries ($\sim$1%), increase abruptly after the explosive summit eruption of 1924 ($\sim$2%), decrease slightly thereafter ($\sim$1%), and remain essentially constant during the late 20th century. These short-term changes in the ^{230}Th–^{238}U disequilibria ($\sim$1–2%) are close to our average analytical uncertainty ($\pm$1.1%) based on repeated Th isotope standard measurements ($\pm$1.1%) and our $\pm$0.3% reproducibility of Th/U ratios. However, we believe these subtle differences are significant because (1) they were verified by duplicate Th isotope ratio measurements for most samples, (2) lavas that erupted during restricted periods of time have extremely constant Th/U, (^{230}Th/^{232}Th), and (^{230}Th/^{238}U) ratios (the 1917 vs. 1919 lavas or the late 20th century lavas; Fig. 2), and (3) duplicate (^{230}Th/^{232}Th) analyses (and recalculated (^{230}Th/^{238}U) ratios) of several samples (1820-1, Kil1919, and six Mauna Ulu and Puu Oo lavas; A. Pietruszka, unpublished data) using new, high-precision plasma ionization multi-collector mass spectrometric (PIMMS) techniques [24] agree within $\sim$0.3% of our TIMS data (Fig. 2). A systematic fluctuation in excess ^{230}Th

[1] http://www.elsevier.nl/locate/epsl; mirrorsite: http://www.elsevier.com/locate/epsl

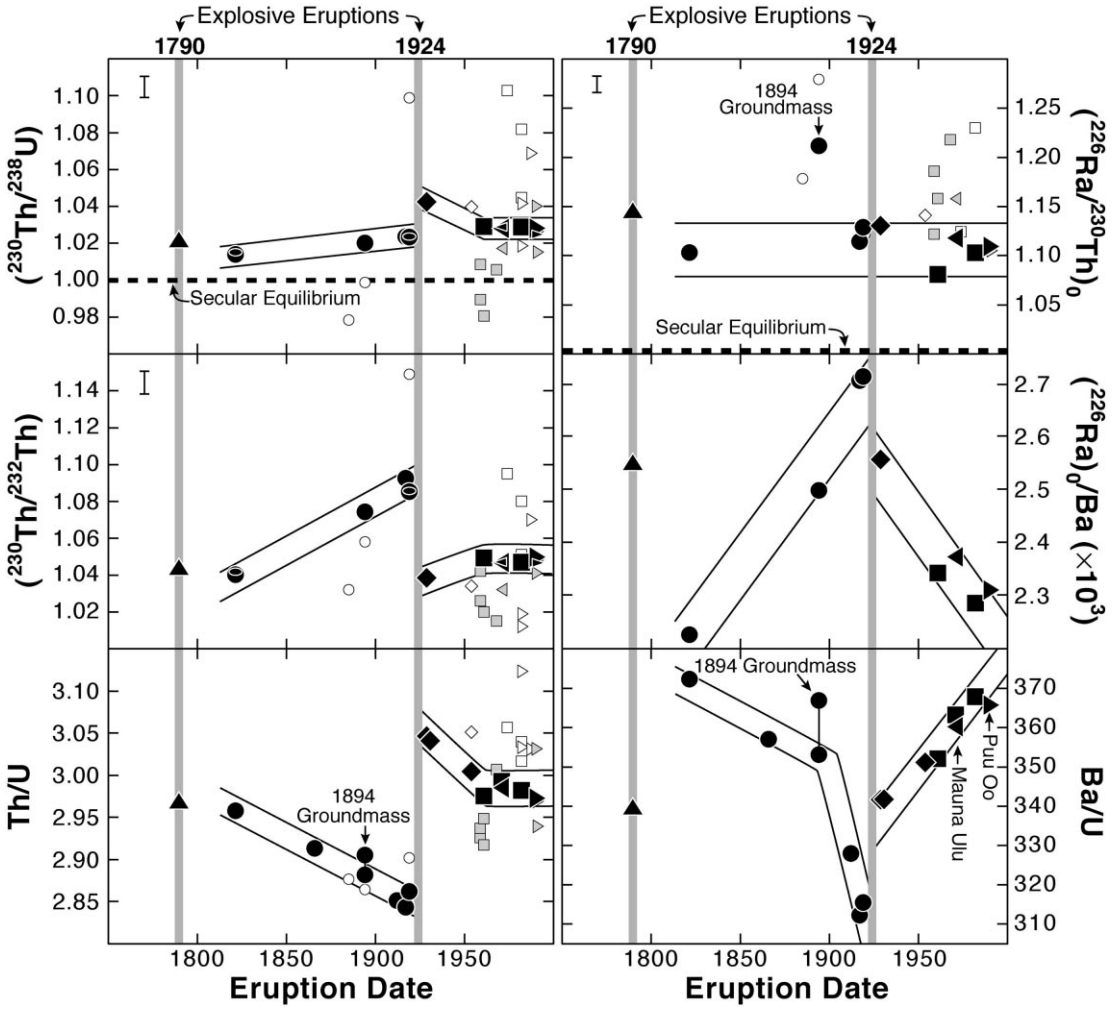

Fig. 2. Temporal variations of U-series isotope and incompatible trace element ratios in Kilauea's historical lavas. The sample symbols are grouped according to eruption date as described in Fig. 1. For comparison with our TIMS data (larger black symbols), duplicate ($^{230}Th/^{232}Th$) analyses (and recalculated ($^{230}Th/^{238}U$) ratios) for several samples using PIMMS (A. Pietruszka, unpublished data) are also shown (smaller black symbols). The black Mauna Ulu and Puu Oo symbols show average values for these rift zone eruptions of Kilauea, which display a relatively narrow range in composition ($\sim$0.3 and 0.8% variation in the amount of excess ^{230}Th, respectively; A. Pietruszka, unpublished data). The other symbols are recent Kilauea literature data collected by TIMS (the gray squares and left triangle are from [16] and the gray, right triangles are from [19,20]) or a combination of TIMS and radioactive decay counting techniques (white symbols; [17]). Our average TIMS $\pm 2\sigma$ error bars are shown on each plot (unless they are smaller than the size of the larger black symbols). The PIMMS ($^{230}Th/^{232}Th$) and ($^{230}Th/^{238}U$) ratios have $\pm 2\sigma$ analytical uncertainties of $\sim$0.2% and 0.3%, respectively (less than or equal to the size of the smaller black symbols).

has not been previously observed in lavas from a Hawaiian shield volcano.

2.2. ^{226}Ra–^{230}Th disequilibria

The ^{226}Ra–^{230}Th disequilibria of Kilauea lavas have also remained relatively constant over the last 200 yr with an 8–15% variation in the amount of excess ^{226}Ra (excluding the 1894 groundmass, which is anomalous; Fig. 2). Compared to other recent studies of Kilauea lavas [16,17], this is a smaller average ^{226}Ra excess and ($^{226}Ra/^{230}Th$)

range (the data of [19] agree with our results of $\sim 12 \pm 4\%$, 2σ). Although the $\sim 7\%$ range in ^{226}Ra–^{230}Th disequilibria observed in this study is significantly greater than our estimate of analytical uncertainty ($\pm 1.4\%$), the samples do not display any systematic temporal trends.

2.3. Th/U, Ba/Th, and Ba/U ratios

Kilauea's historical lavas display significant and systematic temporal variations in their highly incompatible trace element ratios (Fig. 2). The Ba/Th (not shown) and Ba/U ratios decrease from the 19th to early 20th centuries, shift to higher values after the 1924 eruption, and increase during the rest of the 20th century. The Th/U ratios decrease from the 19th to the early 20th centuries, shift suddenly ($\sim 6\%$) after the 1924 eruption from the lowest to the highest values observed in the present study, decrease until the mid-20th century, and remain essentially constant thereafter. The Th/U ratios of historical Kilauea lavas were previously thought to be nearly constant [25].

2.4. ($^{230}Th/^{232}Th$) and (^{226}Ra)/Ba ratios

Kilauea's historical lavas show small, but significant temporal changes in their Th isotope and (^{226}Ra)/Ba ratios (Fig. 2), which have not been previously recognized for lavas from a Hawaiian shield volcano. The ($^{230}Th/^{232}Th$) ratios increase from the 19th to early 20th centuries ($\sim 5\%$), shift abruptly to lower values after the 1924 eruption ($\sim 5\%$), increase slightly towards the mid-20th century ($\sim 1\%$), and remain constant during the late 20th century. The overall ($^{230}Th/^{232}Th$) and (^{226}Ra)/Ba variations mirror (inversely) the temporal changes in the Th/U and Ba/U (or Ba/Th) ratios of the lavas, respectively.

2.5. ($^{234}U/^{238}U$) ratios

All of the samples have ($^{234}U/^{238}U$) ratios that are slightly greater than unity (1.005 on average; Table 1). We do not regard this small deviation from secular equilibrium (not expected for Kilauea's fresh, historical lavas) as significant because the ($^{234}U/^{238}U$) variation is only slightly greater than our analytical uncertainty (± 0.7 vs. $\pm 0.5\%$, respectively) and there is no correlation between the ^{230}Th and apparent ^{234}U excesses. Furthermore, we note that the ($^{234}U/^{238}U$) ratios would be $\sim 0.3\%$ lower if we use the new half-life proposed for ^{234}U [26] instead of the commonly used value in Table 1.

3. Evaluation of post-melting effects on the ^{226}Ra–^{230}Th–^{238}U disequilibria

The main purpose of this study is to use the ^{226}Ra–^{230}Th–^{238}U disequilibria of Kilauea's historical lavas to investigate mantle melting within the Hawaiian plume. However, processes such as radioactive decay or crustal assimilation may have modified the lavas' mantle-derived ($^{226}Ra/^{230}Th$) and ($^{230}Th/^{238}U$) ratios. In this section, we briefly evaluate these possibilities.

3.1. The time scale of magma transport and storage

The compositions of Kilauea's historical summit lavas are controlled mainly by the addition or removal of olivine [27]. However, some of the late 19th–early 20th century lavas have slightly evolved compositions (down to 6.5 wt% MgO for the samples analyzed in this study; M. Garcia, unpublished data) and may also have fractionated small amounts of clinopyroxene and plagioclase. Neither olivine control nor minor clinopyroxene or plagioclase fractionation will directly affect the ^{226}Ra–^{230}Th–^{238}U disequilibria of the lavas (because Ra, Th, and U are thought to be highly incompatible in these minerals [28–34]), but radioactive decay during crystallization may have been important.

The ^{226}Ra excesses of the lavas indicate that the ($^{230}Th/^{238}U$) ratios have not decreased significantly during magma transport and storage. Since the residence time of magma in Kilauea's summit magma reservoir is believed to be much shorter than the half-life of ^{226}Ra (< 80–200 yr during the early 19th to early 20th centuries and 30–40 yr during the late 20th century [35]), the time scale

of magma storage was probably too short to cause a measurable decrease in the (^{226}Ra/^{230}Th) ratios. In contrast, the total duration of magma transport is poorly constrained. Although the transit time from the source to the crust must be significantly less than ~8000 yr in order to preserve the observed, mantle-derived ^{226}Ra–^{230}Th disequilibria [21], the (^{226}Ra/^{230}Th) ratios of the lavas must strictly represent minimum parental magma values.

3.2. Crustal assimilation

One sample, 1894-2, is geochemically anomalous because its microcrystalline groundmass has an elevated (^{226}Ra/^{230}Th) ratio compared to the other historical Kilauea lavas (21% excess ^{226}Ra vs. 12% on average), and much higher Ba/Th (4.7%) and Ba/U (3.9%) and lower Th/Sr (6.3%) and U/Sr (5.6%) than its coexisting glass (Fig. 2 and Table 1). Assuming $D_{Th} = D_U = 0$ and $D_{Sr} = 1.8$ for plagioclase (calculated from [36] with a 1150°C magmatic temperature and a plagioclase composition of An_{75}), ~5.3 wt% plagioclase accumulation accounts for the differences in the Th, U, and Sr concentrations between the groundmass and glass (the lava contains ~5.5 vol% plagioclase-dominated glomerocrysts). However, an unreasonably high plagioclase $D_{Ba} > 1.2$ (assuming $D_{Th} = D_U = D_{Ba} = D_{Sr} = 0$ in olivine, $D_{Th} = D_U = D_{Ba} = 0$ and $D_{Sr} = 0.1$–0.2 in clinopyroxene [29,30]) would be required to explain the Ba signature of the 1894 groundmass by plagioclase accumulation (cf. $D_{Ba} = 0.2$ estimated for plagioclase from [36] as described above). Instead, the relatively high (^{226}Ra/^{230}Th), Ba/Th, and Ba/U ratios of the 1894 groundmass (beyond the minor effect of plagioclase accumulation) probably result from crustal contamination.

The exact mechanism of this contamination at Kilauea is unknown, but assimilation of hydrothermally altered country rock containing young barite [17] or zeolites [37] are two possibilities. Although either scenario might elevate the (^{226}Ra/^{230}Th), Ba/Th, and Ba/U ratios in the magma, secondary zeolites are significantly more common than barite in lavas drilled from Kilauea's active hydrothermal system (D. Thomas, personal communication, 1999). Since the ^{226}Ra excess of the 1894 groundmass may be anomalous due to crustal contamination, we do not use its (^{226}Ra/^{230}Th) ratio in our discussion of mantle melting. The overall ^{226}Ra–^{230}Th disequilibria of the other Kilauea lavas erupted since 1790 are believed to reflect mantle processes, although we cannot rule out the possibility that the small variations in the amount of excess ^{226}Ra (Fig. 2) result from crustal assimilation. However, this will not significantly affect our model results because the melting rates calculated from the (^{226}Ra/^{230}Th) and (^{230}Th/^{238}U) ratios of the lavas are insensitive to subtle differences in the amount of excess ^{226}Ra (Fig. 3).

4. Modeling of mantle melting within the Hawaiian plume

'Instantaneous', or time-independent, melting models (e.g. batch melting [38]) have been invoked previously to explain the incompatible trace element variations of Hawaiian shield lavas [1–4]. Although such models may account for the subtle ^{230}Th excesses of historical Kilauea and Mauna Loa lavas (at melt fractions of ~3–7% [20]), they fail to reproduce the combined ^{226}Ra–^{230}Th–^{238}U disequilibria [17]. Instead, a class of time-dependent models that allow the 'ingrowth' of the short-lived daughter nuclides of ^{238}U during melting are frequently employed (see [39] for a review). A number of 'ingrowth' models have been proposed [10–12,40–42], but we use only the two simplest end members: dynamic melting [10] and equilibrium percolation melting [12]. In this section, we apply these models to the ^{226}Ra–^{230}Th–^{238}U disequilibria of Kilauea's historical lavas and discuss the implications of our model results for mantle melting within the Hawaiian plume.

4.1. 'Ingrowth' melting models and assumptions for Kilauea

Both the dynamic and equilibrium percolation melting models assume that melting occurs at a constant rate in a one-dimensional, steady-state

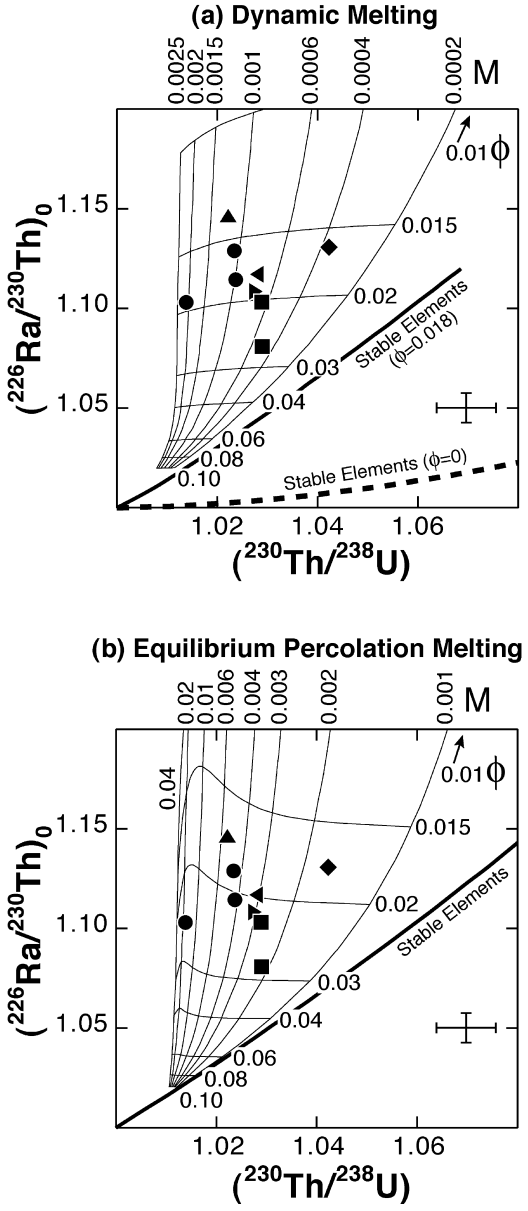

Fig. 3. Melting 'grids' calculated from the (a) dynamic and (b) equilibrium percolation melting models (using the 'Kilauea' D values from Table 2 and a constant melt fraction of 10%) and contoured for different values of melting rate (M: kg m^{-3} yr^{-1}) and melt-zone porosity (ϕ: vol. fraction). For the modeling, similar melting grids were computed to determine the M and ϕ values required to match the ^{226}Ra–^{230}Th–^{238}U disequilibria of each lava (at its particular melt fraction from Fig. 1). This calculation was repeated (for each lava) using the range of partition coefficients from Table 2. For comparison, melting trends for the stable trace element equivalents of the dynamic [11] and equilibrium percolation [12] melting models are also shown. These heavy dashed and solid curves represent the possible ^{226}Ra–^{230}Th–^{238}U disequilibria that can be obtained without the 'ingrowth' of radioactive daughter nuclides (plotted at a range of melt fractions). Our average $\pm 2\sigma$ error bars are shown on each plot. All model calculations assume a 2800 kg m^{-3} liquid density, a 3300 kg m^{-3} solid density, and (for equilibrium percolation melting) that melt is distributed in tubes (permeability exponent = 2). The sample symbols are the same as in Fig. 1. ←

column of upwelling mantle, and that the melt and the residue remain in chemical equilibrium until the melt is extracted. During dynamic melting, all melt in excess of a constant porosity is instantaneously removed from the residue (at all depths of the melting column, simultaneously) and mixed together [10]. In contrast, the melt and residue continuously interact as the melt moves up the melting column during equilibrium percolation melting [12]. For both models, the 'ingrowth' of U-series isotopes (and the creation of ^{226}Ra–^{230}Th–^{238}U disequilibria) is a direct consequence of the greater incompatibility of the shorter-lived daughter nuclide compared to the parent, which leads to different residence times on the melting column for ^{226}Ra, ^{230}Th, and ^{238}U [39]. Excesses of ^{226}Ra and ^{230}Th during dynamic melting arise from a slow rate of melting relative to the half-lives of ^{226}Ra and ^{230}Th, which allow the parent nuclides in the matrix to 'grow' additional daughters and preferentially transfer them to the melt [10]. For equilibrium percolation melting, ^{226}Ra and ^{230}Th excesses arise both from a chromatographic effect in which the daughter nuclides move faster up the melting column than their parents, and from the continuous decay of slower parents to augment their faster daughters [12].

We make the following assumptions for our 'ingrowth' model calculations: (1) the source is in secular equilibrium prior to melting, (2) the height of the melting column is 55 km (~80–135 km deep [43,44]), and (3) melting occurs in the presence of residual garnet [1] with a constant source mineralogy of 60% olivine, 15% clinopyroxene, 15% orthopyroxene, and 10% garnet. In addition, we use estimates for the degree of partial melting at Kilauea (~5–10% [3]; Fig. 1) to ac-

count for any melt fraction effect on the ^{226}Ra–^{230}Th–^{238}U disequilibria. Since the partition coefficients for Ra, Th, and U during mantle melting may vary as a function of pressure, temperature, and composition [31], we also evaluate a range of experimental D values (each combination of D_{Ra} and $D_{Th,U}$ from [28–31,45,46]) and a set of optimal 'Kilauea' partition coefficients chosen from these experiments (Table 2). Given these assumptions (and a few others listed in Fig. 3), we determined the unique combination of melting rate and melt-zone porosity required to match the ($^{226}Ra/^{230}Th$) and ($^{230}Th/^{238}U$) ratios of each lava (at its particular melt fraction from Fig. 1) using the equations for dynamic melting from [11] and a numerical solution to the equations for equilibrium percolation melting [47]. This method is illustrated in Fig. 3.

4.2. Model results

The ^{226}Ra–^{230}Th–^{238}U disequilibria of Kilauea and Mauna Loa lavas have been used previously to quantify the melting parameters for tholeiitic basalt production within the Hawaiian plume [16–19,23]. These studies calculated melting rates of >0.0005–0.01 kg m^{-3} yr^{-1} and melt-zone porosities of <0.1–3% using both the dynamic and equilibrium percolation melting models. We discovered that it was relatively difficult to reproduce the combined ^{226}Ra and ^{230}Th excesses of Kilauea's historical lavas (even though these are among the smallest ^{226}Ra–^{230}Th–^{238}U disequilibria observed in lavas from mid-ocean ridges [21,22] or other ocean island volcanoes [23]) because some combinations of D_{Ra} and $D_{Th,U}$ produced ($^{226}Ra/^{230}Th$) and ($^{230}Th/^{238}U$) ratios that were simply too small or too large. Furthermore, we found that the melting parameters depended strongly (by an order of magnitude or more) on the values of the partition coefficients (Fig. 4). Both of these problems result from the narrow shape of the melting 'grid' for small ^{226}Ra–^{230}Th–^{238}U disequilibria (Fig. 3). Thus, it is difficult to infer a melting rate or porosity solely from the ($^{230}Th/^{238}U$) and ($^{226}Ra/^{230}Th$) ratios of Hawaiian shield lavas. Instead, geological constraints on the melting process are required.

4.3. Melting rate and melt-zone porosity estimates using a geological constraint

The geochemical differences between the adjacent, active Hawaiian volcanoes, Kilauea, Mauna Loa and Loihi (e.g. Pb, Sr, and Nd isotope [4] or Th/U [48] ratios) require that the mantle sources and melting regions of these volcanoes remain physically distinct on the 25–50 km length scale of the distance between them [49]. This idea can potentially be used to constrain the maximum volume of source mantle tapped by Kilauea. Since the rate of magma supply (Q) must be balanced by melting a source volume (V) at a rate (M) such that $Q = V \times M$, the minimum M sampled by this volcano can then be calculated with estimates of Q (from volcanological observations) and this

Table 2
Summary of mineral/liquid partition coefficients

	Clinopyroxene			Garnet		
	Ra	Th	U	Ra	Th	U
B	0.0005	0.0013	0.0009	0.00001	0.0015	0.0096
LaT	–	0.01	0.0045	–	0.0017	0.015
H	0.0058	0.014	0.013	0.00070	0.0014	0.0059
S and L	–	0.005	0.005	–	0.009	0.028
Kil	0.0005	0.005	0.005	0.00001	0.012	0.024

B: Beattie [29,45]. LaT: LaTourrette and Burnett [28]; LaTourrette et al. [46]. H: Hauri et al. [30]. S and L: Salters and Longhi [31]. Kil: 'Kilauea' partition coefficients from [29,45] for D_{Ra} in clinopyroxene and garnet, [31] for D_{Th} and D_U in clinopyroxene, and a single experiment of [31] for D_{Th} and D_U in garnet. Partition coefficients for Ra have never been measured, but D_{Ra} is probably less than D_{Ba} in these minerals due to the larger ionic radius of Ra [34]. We assume $D_{Ra} = D_{Ba}$ for simplicity, but evaluate a range of values. The D values for Ra (= Ba), Th, and U in olivine and orthopyroxene are expected to be extremely low [29] and are assumed to be zero.

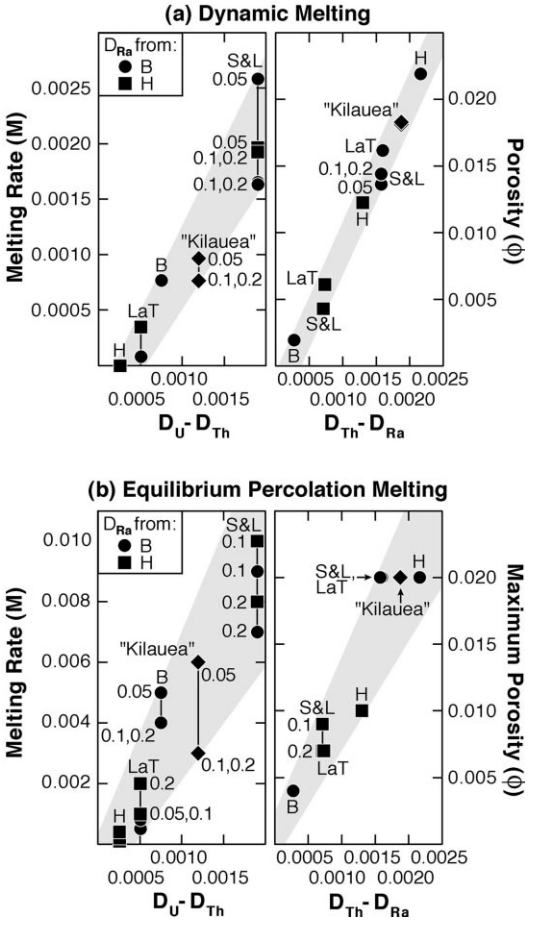

Fig. 4. Melting rates and melt-zone porosities calculated from the (a) dynamic and (b) equilibrium percolation melting models using a range of bulk partition coefficients for Ra, Th, and U. The values plotted are those that best match the average ($^{226}Ra/^{230}Th$) and ($^{230}Th/^{238}U$) ratios of our data at melt fractions of 5, 10, and 20%. The literature sources of the partition coefficients used for each calculation are indicated on the figure (symbols for D_{Ra} and letter codes for $D_{Th,U}$ keyed to Table 2). The melt fractions (small numbers) are shown only for those parameterizations that display a significant change of melting rate or porosity as a function of melt fraction. Some combinations of D_{Ra} and $D_{Th,U}$ produced ^{226}Ra–^{230}Th–^{238}U disequilibria that were simply too small (e.g. the '*H*' values of $D_{Th,U}$ from [30] for both 'ingrowth' melting models) or too large (e.g. the '*S* and *L*' values of $D_{Th,U}$ from [31] for equilibrium percolation melting at melt fractions of 5%) to account for the average ^{226}Ra–^{230}Th–^{238}U disequilibria of the lavas. In these cases, approximate values are shown (if possible).

maximum estimate of V (from the intershield geochemical differences).

To apply this geological constraint, we assume that Kilauea taps a cylindrical volume of source mantle with a height of 55 km (~135–80 km deep; Fig. 5), which is thought to represent the maximum vertical extent of the melting region on the axis of the Hawaiian plume [43,44]. For this geometry, the radius of Kilauea's melting column (a relatively small portion of the much wider up-

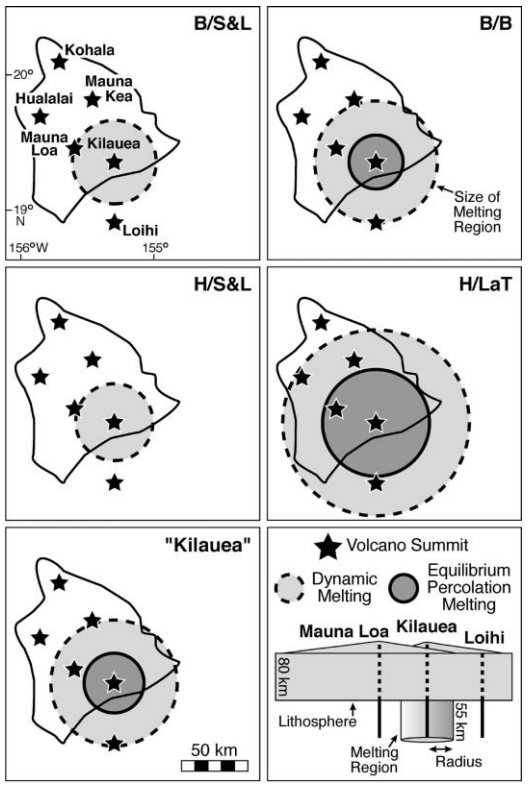

Fig. 5. Maximum source volumes for historical Kilauea lavas estimated from the dynamic and equilibrium percolation melting models using a range of partition coefficients for Ra, Th, and U. Ideally, the radii of these hypothetical source volumes (plotted on each map assuming a cylindrical melt-column geometry with a maximum height of 55 km [43,44]) should be less than half the distance between Kilauea, Mauna Loa and Loihi in order to preserve their geochemical differences. The letter codes in each plot refer to the literature source of the values used for D_{Ra} and $D_{Th,U}$, respectively (Table 2). The results of this calculation are shown only for those sets of partition coefficients that successfully reproduce the observed range of ^{226}Ra–^{230}Th–^{238}U disequilibria. See the text for more details.

welling plume) should ideally be less than half the distance between the three active volcanoes in order to preserve the distinct geochemical signature of Kilauea lavas. If we use a more conservative radial limit of 25 km (~75% of the distance between the summits of Kilauea and Mauna Loa), the maximum volume of source mantle sampled by Kilauea would be $\sim 1.1\times10^5$ km^3.

Residence time analysis of the geochemical fluctuations observed in historical Kilauea lavas suggests that the volume of magma within the volcano's summit magma storage reservoir has remained essentially constant since 1790 [35]. For such a steady-state volcanic system, the eruption rate may be used as a proxy for the magma supply rate. Combining our best estimates of Q (from the eruption rates in Fig. 1) with the maximum V of $\sim 1.1\times10^5$ km^3 results in minimum M for Kilauea (assuming a 2800 kg m^{-3} melt density) that ranges from >0.0001 kg m^{-3} yr^{-1} during periods of low magma supply (e.g. after the 1924 eruption) to >0.003 kg m^{-3} yr^{-1} during periods of high magma supply (e.g. 1790, the early 19th century, and the Puu Oo eruption).

To be successful, our 'ingrowth' model calculations must be consistent with these minimum melting rates. In other words, the combination of Q (from Fig. 1) and M (inferred from a given parameterization of either 'ingrowth' model) for each lava must result in a V that is small enough to satisfy the geological constraint from the inter-shield geochemical differences. Thus, we determined a V for each lava (for each combination of D_{Ra} and $D_{Th,U}$ from Table 2) using the melting rate inferred from its (^{226}Ra/^{230}Th) and (^{230}Th/^{238}U) ratios (at its particular melt fraction; Fig. 1) and our best estimate of the volcano's magma supply rate at the time of its eruption (Fig. 1). For each set of partition coefficients, this calculation results in a range of V values that reflect the different values of Q and M used for each lava. Radii were calculated from these source volumes as described above. For comparison, the largest melt-column radius for each set of partition coefficients that reproduced the observed range of ^{226}Ra–^{230}Th–^{238}U disequilibria is plotted on a map of the Island of Hawaii (Fig. 5).

In all cases, the maximum melt-column radii

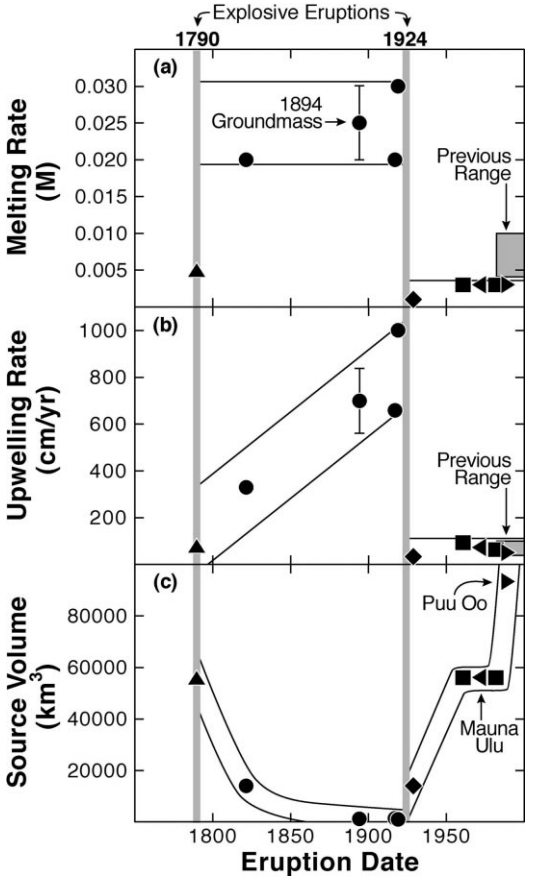

Fig. 6. Temporal variations of (a) melting rate, (b) upwelling rate, and (c) source volume inferred from Kilauea's historical summit lavas. The melting rates are calculated to match the (^{226}Ra/^{230}Th) and (^{230}Th/^{238}U) ratios of each sample using the equilibrium percolation model, the 'Kilauea' D values from Table 2, and melt fractions from Fig. 1. The upwelling rates and source volumes are estimated from these melting rates as described in the text. The range in these parameters for the 1894 groundmass was calculated using our total observed variation of ^{226}Ra–^{230}Th disequilibria for Kilauea, rather than the (^{226}Ra/^{230}Th) ratio of this sample (which may be elevated due to crustal contamination). The previous ranges for these melting parameters based on Puu Oo lavas are from [19]. The symbols are the same as in Fig. 1.

are similar to or significantly larger than half the distance between the three active volcanoes. Even if we use the more conservative radial limit of 25 km, only two sets of Ra, Th, and U partition coefficients (the values of [29,45], and the optimal 'Kilauea' D values from [29,45] for D_{Ra}

and [31] for $D_{Th,U}$) with the equilibrium percolation melting model satisfy the geological constraint. Since the Th and U partition coefficients of [31] are thought to be more appropriate for the melting of garnet peridotite, we use the 'Kilauea' D values (and the equilibrium percolation melting model) for the remainder of the discussion.

Thus, our best estimates of the melting parameters for tholeiitic basalt production within the Hawaiian plume (as tapped by Kilauea) are a melt-zone porosity of $\sim$2% and melting rates of $\sim$0.003–0.03 kg m^{-3} yr^{-1} (excluding a relatively low melting rate of $\sim$0.001 kg m^{-3} yr^{-1} inferred from the 1929 lava, which is geochemically anomalous [3]; Fig. 2). This porosity estimate is similar to the highest values previously inferred from Kilauea and Mauna Loa lavas ($\sim$2–3% [19]), although it must strictly represent a maximum value (because of ^{226}Ra decay during magma transport and storage). In contrast, our calculated melting rates range to significantly higher values than previous estimates for Hawaiian shield volcanoes ($>$0.0005–0.01 kg m^{-3} yr^{-1} [16–19,23]).

Interestingly, our 'ingrowth' model results also suggest that Kilauea lavas from the 19th to early 20th centuries were produced at systematically higher rates of mantle melting than lavas from 1790 and the late 20th century ($\sim$0.02–0.03 vs. 0.003–0.005 kg m^{-3} yr^{-1}, respectively; Fig. 6a). This shift derives mostly from the smaller ^{230}Th–^{238}U disequilibria of the 19th–early 20th century lavas (at a given melt fraction; Fig. 7). The absolute range in the melting rate at Kilauea is difficult to quantify independently, but our calculations using the geological constraint from the inter-shield geochemical differences suggest that relatively high $M\geq$0.003 kg m^{-3} yr^{-1} (regardless of any 'ingrowth' model assumptions or choice of partition coefficients) are required during periods of high magma supply (e.g. 1790 and the Puu Oo eruption). The 19th–early 20th century lavas may have formed at much higher melting rates (up to a factor of $\sim$10) even though their (^{230}Th/^{238}U) ratios are only slightly lower because both 'ingrowth' models predict that large changes in the rate of mantle melting (at the high M appropriate for Kilauea) are required to cause even a subtle shift in the amount of excess ^{230}Th (Fig. 7).

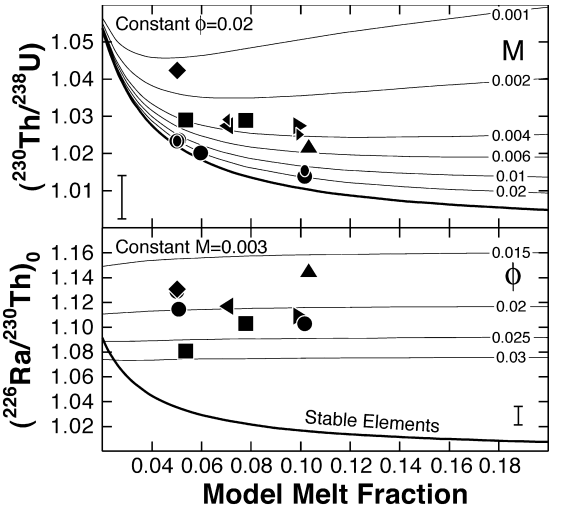

Fig. 7. The effect of melt fraction on ^{226}Ra–^{230}Th–^{238}U disequilibria calculated from the equilibrium percolation melting model (using the 'Kilauea' D values from Table 2) and contoured for different values of melting rate (M) or melt-zone porosity (ϕ). The constant M and ϕ values indicated in the upper left corners of the plots are the melting parameters that best match the average (^{226}Ra/^{230}Th) and (^{230}Th/^{238}U) ratios of our data. For comparison, the melting trend for the stable trace element equivalent of the equilibrium percolation melting model [12] is also shown. The melt fraction estimates are from Fig. 1. The larger black symbols (TIMS data) are the same as in Fig. 1. The average TIMS $\pm 2\sigma$ error bars are shown on each plot. The smaller black symbols are recalculated (^{230}Th/^{238}U) ratios using high-precision PIMMS (^{230}Th/^{232}Th) analyses (A. Pietruszka, unpublished data). The PIMMS (^{230}Th/^{238}U) ratios have $\pm 2\sigma$ analytical uncertainties of $\sim$0.3% (similar to the size of the smaller symbols).

Although this wide range is model-dependent, we believe that the relative differences in M between these periods are significant because (1) similar results (of different magnitude) are obtained using both 'ingrowth' models with all combinations of D_{Ra} and $D_{Th,U}$ that reproduce the observed range of ^{226}Ra–^{230}Th–^{238}U disequilibria (the parameterizations shown on Fig. 5) and (2) they correlate with the changes in the trajectory of the temporal geochemical variations that follow the two major explosive eruptions at the summit of the volcano in 1790 and 1924 (Fig. 2; [3]). However, we also evaluate the possibility that the apparent differences in M result from an incorrect model assumption.

4.4. The effect of melt fraction

Kilauea's historical lavas display a systematic temporal fluctuation of incompatible trace element ratios (e.g. La/Yb or Nb/Y) that is thought to result from a rapid change in the degree of partial melting at this volcano over the last 200 yr [3]. Our previous 'instantaneous' (batch) melting model calculations based on these geochemical variations (Fig. 1) suggest that the melt fraction at Kilauea decreased by a factor of ~2 (~10–5%) from the 19th to mid-20th century, and subsequently increased towards the present (again by a factor of ~2). These melt fraction estimates are compatible with the 'ingrowth' melting models because the geochemical effects of dynamic melting (at melt fractions above ~5% and relatively high porosities) and equilibrium percolation melting for stable trace elements are similar [11] or identical [12] to batch melting, respectively. Although the relative (factor of ~2) difference in the degree of partial melting that we use for our 'ingrowth' model calculations is probably accurate, the absolute values are model-dependent [3]. However, incorrect, assumed melt fractions cannot account for the range in melting rates because neither 'ingrowth' model predicts a strong relationship between ^{226}Ra–^{230}Th–^{238}U disequilibria and melt fraction (over the ~5–20% range expected for Hawaiian shield lavas [50]; Fig. 7). At most, the decrease in the degree of partial melting from the 19th to mid-20th century may explain the subtle (~1%) increase in the (^{230}Th/^{238}U) ratios of the lavas erupted during this period, which plot along a line of nearly constant M (Fig. 7). Even if we assume a constant melt fraction (despite the trace element evidence to the contrary [3]), the M inferred from the 19th–early 20th century lavas would still be relatively high due to their subtly lower (^{230}Th/^{238}U) ratios (e.g. melting 'grid' at a constant 10% melt fraction; Fig. 3).

4.5. The role of source heterogeneity

The short-term fluctuation in melt fraction at Kilauea since 1790 correlates with an overall change in the mantle source composition (or proportion of source components; Fig. 1). The source that was preferentially tapped during the early 20th century (when melt fractions were lowest) corresponds to the 'Kilauea' isotopic end member for Hawaiian volcanoes (characterized by relatively low ^{87}Sr/^{86}Sr, and high ε_{Nd} and ^{206}Pb/^{204}Pb), which is thought to represent a long-term depleted component within the Hawaiian plume [3]. The relatively high (^{230}Th/^{232}Th) and (^{226}Ra)/Ba, and low Ba/U, Ba/Th, and Th/U ratios of the early 20th century lavas compared to other Kilauea (Fig. 1 and Table 1) and historical Mauna Loa lavas [16–20] suggest that this 'Kilauea' source component is also more depleted in highly incompatible trace elements at the present time (compared to the source of the early 19th and late 20th century Kilauea or historical Mauna Loa lavas). A simple explanation for this inverse relationship between the magnitude of source depletion and melt fraction (Fig. 1) is that source fertility (i.e. lithology) controls the degree of partial melting at Kilauea. For example, the (more depleted) source of the early 20th century lavas might have a relatively high solidus temperature, which would prevent it from melting as much as the (less depleted) source of the early 19th and late 20th century lavas.

The results of the 'ingrowth' melting models for ^{226}Ra–^{230}Th–^{238}U disequilibria are independent of the mantle source composition (e.g. Th/U ratio) as long as the source is in secular equilibrium prior to melting [10–12]. However, melting a lithologically heterogeneous source in variable proportions might cause the (^{230}Th/^{238}U) ratios of lavas to vary if the bulk Th and U partition coefficients are different for each component [51,52]. The magnitude of this effect depends mostly on the relative abundances of garnet since this is the mineral typically expected to create significant ^{230}Th excesses during mantle melting [28–31,45,46]. Indeed, a mixed source lithology has been proposed for Hawaiian lavas (garnet-poor peridotite vs. garnet-rich pyroxenite or eclogite) based on a correlation between their ^{230}Th–^{238}U disequilibria and Th/U ratios [52] and other geochemical evidence [53,54].

However, the overall ^{230}Th excesses of Kilauea's historical lavas do not correlate with either

their (^{230}Th/^{232}Th) or Th/U ratios (compare plots in Fig. 2), or any other tracer of mantle source composition (cf. [3]). Even the well defined trend towards the 'Kilauea' end member from the 19th to early 20th centuries is characterized by a subtle increase in (^{230}Th/^{238}U), which is opposite to the relationship expected from melting a more depleted, garnet-poor source over time. If source fertility controls the degree of partial melting at Kilauea (as we propose), the lithological heterogeneity must be dominated by differences in the abundance of clinopyroxene (rather than garnet and clinopyroxene). This could provide the necessary difference in solidus temperature with little effect on the ^{230}Th–^{238}U disequilibria (due to the general similarity of Th and U partition coefficients for this mineral [28–31,45,46]). The only possible exception to this scenario comes from the geochemically anomalous lavas erupted just after 1924, which have relatively high (^{230}Th/^{238}U) and Th/U and low (^{230}Th/^{232}Th) ratios (Fig. 2) and may have tapped a source that was less depleted and richer in garnet than the source of the early 20th century lavas. In any case, source heterogeneity cannot account for the range in melting rates.

4.6. The importance of the melt-column height

Our 'ingrowth' model calculations assume a constant melt-column height (d) for Kilauea. Alternately, it is possible that d is variable. However, the melting rate inferred from the (^{226}Ra/^{230}Th) and (^{230}Th/^{238}U) ratios of a lava (for a constant source mineralogy) is independent of the melt-column height for both dynamic melting (because d is not a parameter in the equations [11]) and equilibrium percolation melting (because d cancels out of the equations [12] for melts leaving the top of the melting column). Thus, variations in d cannot explain the differences in M.

4.7. The dynamics of mantle melting at Kilauea

Based on our evaluation of the 'ingrowth' model parameters, an incorrect assumption is unlikely to account for the range in melting rates inferred from the ^{226}Ra–^{230}Th–^{238}U disequilibria of Kilauea's historical lavas. To explore the implications of these differences in M, we converted our best estimates of the rate of mantle melting at this volcano since 1790 (from Fig. 6a) to upwelling rates (W) using the relationship $W = M \times d/\rho_s \times F$ from [14], where d is the melt-column height (55 km), ρ_s is the solid density (3300 kg m^{-3}) and F is the melt fraction from Fig. 1. This calculation (Fig. 6b) suggests that Kilauea lavas from the 19th to early 20th centuries were derived from mantle that was upwelling significantly faster than the mantle that melted to form the lavas from 1790 and the late 20th century ($\sim$300–1000 vs. 50–90 cm yr^{-1}, respectively). These upwelling rates range to significantly higher values than previous estimates for Hawaiian shield volcanoes (40–100 cm yr^{-1} [19]). Although the wide variation (up to a factor of $\sim$10) is model-dependent, we believe that the relative differences in W between these periods are significant for the same reasons as the range in melting rates. Even if we assume that (1) the melt fraction is constant (despite the trace element evidence to the contrary [3]) or (2) the melt-column height varies in proportion to the degree of partial melting (i.e. a constant melt productivity, F/d), the W inferred from the 19th–early 20th century lavas would still be relatively high due to their higher M.

Fluid dynamical models predict an exponential increase in the rate of mantle upwelling (and, thus, the rate of melting) towards the core of the Hawaiian plume (up to 1000 cm yr^{-1} [43,44,55]). This basic pattern of W and M has been verified using measurements of U-series isotope disequilibria in zero-age, spatially dispersed Hawaiian lavas [19]. The range in the melting parameters (both M and W) at Kilauea since 1790 can also be explained in the context of this model if (1) this volcano taps the center of the plume (in contrast to previous suggestions [8,53]) where W and M are expected to be the highest and the most variable and (2) the volume (and radius) of the melting region sampled by the volcano changes on a time scale of years to decades. For example, the 19th–early 20th century lavas may have been derived by melting a narrow region near the core of the plume (at the highest M and W), whereas the lavas from 1790 and the

late 20th century may have been derived by melting a wider area of the plume (at lower M and W on average).

Indeed, our 'ingrowth' model results suggest that the volume of the melting region sampled by Kilauea has changed significantly since 1790 (Fig. 6c) with a short-term decrease during the 19th to early 20th centuries (calculated from the relationship $Q = V \times M$ using our best estimates of Q from Fig. 1 and M from Fig. 6a). Assuming a cylindrical melting region with a constant height, these differences in V translate directly to differences in the melt-column radius. Smaller source volumes (and radii) for the 19th–early 20th century lavas are obtained even if we assume a smaller range of M and/or a variable melt-column height (i.e. a constant melt productivity, F/d) because the volcano's eruption rate (and, presumably, its magma supply rate) was significantly lower during this period (Fig. 1). In general, lavas that formed at relatively high M and W derive from smaller volumes (and radii) of source mantle and vice versa (compare plots in Fig. 6), which is consistent with the fluid dynamical models of the Hawaiian plume [43,44,55].

The smallest source volumes were tapped by Kilauea during the early 20th century when the volcano erupted lavas with Pb, Sr, and Nd isotope ratios that correspond to the 'Kilauea' end member for Hawaiian volcanoes [3], whereas lavas derived from the largest source volumes (such as those from the Puu Oo eruption) overlap isotopically with recent Loihi tholeiitic basalts [4]. This behavior probably results from the more effective blending of small-scale heterogeneities within the Hawaiian plume as the melting region sampled by Kilauea increases in size (e.g. [5]). Thus, rapid changes in the size of the melting region tapped by the volcano (in the presence of these heterogeneities) may regulate most of the source- and melting-related geochemical variations at Kilauea over time scales of decades to centuries.

5. Conclusions

In this study, we have used high-precision measurements of the U-series isotope abundances of Kilauea's historical lavas (in conjunction with Pb, Sr, and Nd isotope ratios and incompatible trace elements) to examine the process of melt generation at this volcano. Our results show that the ^{226}Ra–^{230}Th–^{238}U disequilibria of these lavas have remained relatively small and constant since 1790 with $\sim 12 \pm 4\%$ excess ^{226}Ra and $\sim 2.5 \pm 1.6\%$ excess ^{230}Th (both are $\pm 2\sigma$). Model calculations based mostly on subtle variations in the ($^{230}Th/^{238}U$) ratios suggest that Kilauea lavas from the 19th to early 20th centuries formed at significantly higher rates of mantle melting and upwelling (up to a factor of ~ 10) compared to lavas from 1790 and the late 20th century. These differences in M and W cannot be explained by analytical error or by an incorrect model assumption. The shift to higher values for these parameters correlates with a short-term decrease in the size of the melting region sampled by the volcano, which is consistent with fluid dynamical models that predict an exponential increase in the upwelling rate (and, thus, the melting rate) towards the core of the Hawaiian plume. The Pb, Sr, and Nd isotope ratios of lavas derived from the smallest source volumes correspond to the 'Kilauea' end member of Hawaiian volcanoes, whereas lavas that tapped the largest source volumes overlap isotopically with recent Loihi tholeiitic basalts. This behavior probably arises from the more effective blending of small-scale source heterogeneities as the melting region sampled by Kilauea increases in size. The source that was preferentially tapped during the early 20th century (when the melt fractions were lowest) is more chemically and isotopically depleted than the source of the early 19th and late 20th century lavas (which formed by the highest melt fractions). This inverse relationship between the magnitude of source depletion and melt fraction suggests that source fertility (i.e. lithology) controls the degree of partial melting at Kilauea. Thus, rapid changes in the size of melting region tapped by the volcano (in the presence of these small-scale heterogeneities) may regulate most of the source- and melting-related geochemical variations at Kilauea over time scales of decades to centuries.

Acknowledgements

We thank M. Spiegelman for stimulating discussions about equilibrium percolation melting and help with his 'Usercalc' program, A. Hofmann for sharing his unpublished Mauna Ulu Pb isotope data, K. Spencer for his skilled maintenance of the Hawaii isotope lab, L. Sacks for help with the 'unspiked' analysis of Kil1919, and K. Sims for a helpful review. We greatly appreciated the assistance of R. Muse, K. Kolysko-Rose, and M. Ito with the preparation of the samples for chemical analysis. This work was supported by NSF Grants EAR 9628288 (to K.R.) and 9614247 and 0001123 (to M.G.). This is SOEST Contribution #5301. *[FA]*

References

[1] A.W. Hofmann, M.D. Feigenson, I. Raczek, Case studies on the origin of basalt, III, Petrogenesis of the Mauna Ulu eruption, Kilauea, 1969–1971, Contrib. Mineral. Petrol. 88 (1984) 24–35.

[2] J.M. Rhodes, S.R. Hart, Episodic trace element and isotopic variations in historical Mauna Loa lavas: implications for magma and plume dynamics, in: J.M. Rhodes, J.P. Lockwood (Eds.), Mauna Loa Revealed: Structure, Composition, History, and Hazards, AGU, Geophys. Monogr. 92, 1995, pp. 263–288.

[3] A.J. Pietruszka, M.O. Garcia, A rapid fluctuation in the mantle source and melting history of Kilauea Volcano inferred from the geochemistry of its historical summit lavas (1790–1982), J. Petrol. 40 (1999) 1321–1342.

[4] M.O. Garcia, A.J. Pietruszka, J.M. Rhodes, K. Swanson, Magmatic processes during the prolonged Puu Oo eruption of Kilauea Volcano, Hawaii, J. Petrol. 41 (2000) 967–990.

[5] M.D. Norman, M.O. Garcia, Primitive magmas and source characteristics of the Hawaiian plume: petrology and geochemistry of shield picrites, Earth Planet. Sci. Lett. 168 (1999) 27–44.

[6] M.D. Kurz, T.C. Kenna, D.P. Kammer, J.M. Rhodes, M.O. Garcia, Isotopic evolution of Mauna Loa Volcano: a view from the submarine southwest rift zone, in: J.M. Rhodes, J.P. Lockwood (Eds.), Mauna Loa Revealed: Structure, Composition, History, and Hazards, AGU, Geophys. Monogr. 92, 1995, pp. 289–306.

[7] F. Albarède, High-resolution geochemical stratigraphy of Mauna Kea flows from the Hawaii Scientific Drilling Project core, J. Geophys. Res. 101 (1996) 11841–11853.

[8] J.C. Lassiter, D.J. DePaolo, M. Tatsumoto, Isotopic evolution of Mauna Kea Volcano: results from the initial phase of the Hawaii Scientific Drilling Project, J. Geophys. Res. 101 (1996) 11769–11780.

[9] V.M. Oversby, P.W. Gast, Lead isotope compositions and uranium decay series disequilibrium in recent volcanic rocks, Earth Planet. Sci. Lett. 5 (1968) 199–206.

[10] D. McKenzie, ^{230}Th–^{238}U disequilibrium and the melting processes beneath ridge axes, Earth Planet. Sci. Lett. 72 (1985) 149–157.

[11] R.W. Williams, J.B. Gill, Effects of partial melting on the uranium decay series, Geochim. Cosmochim. Acta 53 (1989) 1607–1619.

[12] M. Spiegelman, T. Elliott, Consequences of melt transport for uranium series disequilibrium in young lavas, Earth Planet. Sci. Lett. 118 (1993) 1–20.

[13] S. Krishnaswami, K.K. Turekian, J.T. Bennett, The behavior of ^{232}Th and the ^{238}U decay chain nuclides during magma formation and volcanism, Geochim. Cosmochim. Acta 48 (1984) 505–511.

[14] S. Newman, R.C. Finkel, J.D. Macdougall, Comparison of ^{230}Th–^{238}U disequilibrium systematics in lavas from three hot spot regions: Hawaii, Prince Edward and Samoa, Geochim. Cosmochim. Acta 48 (1984) 315–324.

[15] I.M. Reinitz, K.K. Turekian, The behavior of the uranium decay chain nuclides and thorium during the flank eruptions of Kilauea (Hawaii) between 1983 and 1985, Geochim. Cosmochim. Acta 55 (1991) 3735–3740.

[16] A.S. Cohen, R.K. O'Nions, Melting rates beneath Hawaii: evidence from uranium series isotopes in recent lavas, Earth Planet. Sci. Lett. 120 (1993) 169–175.

[17] C. Hémond, A.W. Hofmann, G. Heusser, M. Condomines, I. Raczek, J.M. Rhodes, U–Th–Ra systematics in Kilauea and Mauna Loa basalts, Hawaii, Chem. Geol. 116 (1994) 163–180.

[18] A.S. Cohen, R.K. O'Nions, M.D. Kurz, Chemical and isotopic variations in Mauna Loa tholeiites, Earth Planet. Sci. Lett. 143 (1996) 111–124.

[19] K.W.W. Sims, D.J. DePaolo, M.T. Murrell, W.S. Baldridge, S. Goldstein, D. Clague, M. Jull, Porosity of the melting zone and variations in the solid mantle upwelling rate beneath Hawaii: inferences from the ^{238}U–^{230}Th–^{226}Ra and ^{235}U–^{231}Pa disequilibria, Geochim. Cosmochim. Acta 63 (1999) 4119–4138.

[20] K.W.W. Sims, D.J. DePaolo, M.T. Murrell, W.S. Baldridge, S.J. Goldstein, D.A. Clague, Mechanisms of magma generation beneath Hawaii and mid-ocean ridges: uranium/thorium and samarium/neodymium isotopic evidence, Science 267 (1995) 508–512.

[21] K.H. Rubin, J.D. Macdougall, ^{226}Ra excesses in mid-ocean-ridge basalts and mantle melting, Nature 335 (1988) 158–161.

[22] A.M. Volpe, S.J. Goldstein, ^{226}Ra–^{230}Th disequilibrium in axial and off-axis mid-ocean ridge basalts, Geochim. Cosmochim. Acta 57 (1993) 1233–1241.

[23] F. Chabaux, C.J. Allègre, ^{238}U–^{230}Th–^{226}Ra disequilibria in volcanics: a new insight into melting conditions, Earth Planet. Sci. Lett. 126 (1994) 61–74.

[24] A.J. Pietruszka, R.W. Carlson, E.H. Hauri, Accurate and

precise measurement of U-series disequilibria in volcanic rocks by plasma ionization multicollector mass spectrometry (PIMMS), EOS Trans. AGU, 2000, p. 422.
[25] K.P. Jochum, A.W. Hofmann, Contrasting Th/U in historical Mauna Loa and Kilauea lavas, in: J.M. Rhodes, J.P. Lockwood (Eds.), Mauna Loa Revealed: Structure, Composition, History, and Hazards, AGU, Geophys. Monogr. 92, 1995, pp. 307–314.
[26] H. Cheng, R.L. Edwards, J. Hoff, C.D. Gallup, D.A. Richards, Y. Asmerom, The half-lives of uranium-234 and thorium-230, Chem. Geol. 169 (2000) 17–33.
[27] T.L. Wright, Chemistry of Kilauea and Mauna Loa in space and time, U.S. Geol. Surv. Prof. Pap. 735 (1971) 1–40.
[28] T.Z. LaTourrette, D.S. Burnett, Experimental determination of U and Th partitioning between clinopyroxene and natural and synthetic basaltic liquid, Earth Planet. Sci. Lett. 110 (1992) 227–244.
[29] P. Beattie, The generation of uranium series disequilibria by partial melting of spinel peridotite: constraints from partitioning studies, Earth Planet. Sci. Lett. 117 (1993) 379–391.
[30] E.H. Hauri, T.P. Wagner, T.L. Grove, Experimental and natural partitioning of Th, U, Pb and other trace elements between garnet, clinopyroxene and basaltic melts, Chem. Geol. 117 (1994) 149–166.
[31] V.J.M. Salters, J. Longhi, Trace element partitioning during the initial stages of melting beneath mid-ocean ridges, Earth Planet. Sci. Lett. 166 (1999) 15–30.
[32] W.C. Phinney, D.A. Morrison, Partition coefficients for calcic plagioclase: implications for Archean anorthosites, Geochim. Cosmochim. Acta 54 (1990) 1639–1654.
[33] P. Henderson, Inorganic Geochemistry, Pergamon Press, New York, 1982, 353 pp.
[34] J. Blundy, B. Wood, Prediction of crystal-melt partition coefficients from elastic moduli, Nature 372 (1994) 452–454.
[35] A.J. Pietruszka, M.O. Garcia, The size and shape of Kilauea Volcano's summit magma storage reservoir: a geochemical probe, Earth Planet. Sci. Lett. 167 (1999) 311–320.
[36] J.D. Blundy, B.J. Wood, Crystal-chemical controls on the partitioning of Sr and Ba between plagioclase feldspar, silicate melts, and hydrothermal solutions, Geochim. Cosmochim. Acta 55 (1991) 193–209.
[37] N.C. Sturchio, J.K. Bohlke, C.M. Binz, Radium–thorium disequilibrium and zeolite–water ion exchange in a Yellowstone hydrothermal environment, Geochim. Cosmochim. Acta 53 (1989) 1025–1034.
[38] D.M. Shaw, Trace element fractionation during anatexis, Geochim. Cosmochim. Acta 34 (1970) 237–243.
[39] T. Elliott, Fractionation of U and Th during mantle melting: a reprise, Chem. Geol. 139 (1997) 165–183.
[40] Z. Qin, Disequilibrium partial melting model and its implications for trace element fractionations during mantle melting, Earth Planet. Sci. Lett. 112 (1992) 75–90.
[41] H. Iwamori, ^{238}U–^{230}Th–^{226}Ra and ^{235}U–^{231}Pa disequilibria produced by mantle melting with porous and channel flows, Earth Planet. Sci. Lett. 125 (1994) 1–16.
[42] C. Richardson, D. McKenzie, Radioactive disequilibria from 2D models of melt generation by plumes and ridges, Earth Planet. Sci. Lett. 128 (1994) 425–437.
[43] S. Watson, D. McKenzie, Melt generation by plumes: a study of Hawaiian volcanism, J. Petrol. 32 (1991) 501–537.
[44] N.M. Ribe, U.R. Christensen, The dynamical origin of Hawaiian volcanism, Earth Planet. Sci. Lett. 171 (1999) 517–531.
[45] P. Beattie, Uranium–thorium disequilibria and partitioning on melting of garnet peridotite, Nature 363 (1993) 63–65.
[46] T.Z. LaTourrette, A.K. Kennedy, G.J. Wasserburg, Thorium–uranium fractionation by garnet evidence for a deep source and rapid rise of oceanic basalts, Science 261 (1993) 739–742.
[47] M. Spiegelman, UserCalc: a web-based uranium series calculator for magma migration problems, Geochem. Geophys. Geosyst. 1, 2000, 1999GC000030.
[48] M.O. Garcia, K.H. Rubin, M.D. Norman, J.M. Rhodes, D.W. Graham, D.W. Muenow, K. Spencer, Petrology and geochronology of basalt breccia from the 1996 earthquake swarm of Loihi seamount, Hawaii: magmatic history of its 1996 eruption, Bull. Volcanol. 59 (1998) 577–592.
[49] F.A. Frey, J.M. Rhodes, Intershield geochemical differences among Hawaiian volcanoes: implications for source compositions, melting process and magma ascent paths, Phil. Trans. R. Soc. London 342 (1993) 121–136.
[50] S. Watson, Rare earth element inversions and percolation models for Hawaii, J. Petrol. 34 (1993) 763–783.
[51] C.C. Lundstrom, Q. Williams, J.B. Gill, Investigating solid mantle upwelling rates beneath mid-ocean ridges using U-series disequilibria, 1: a global approach, Earth Planet. Sci. Lett. 157 (1998) 151–165.
[52] O. Sigmarsson, S. Carn, J.C. Carracedo, Systematics of U-series nuclides in primitive lavas from the 1730-36 eruption on Lanzarote, Canary Islands, and implications for the role of garnet pyroxenites during oceanic basalt formations, Earth Planet. Sci. Lett. 162 (1998) 137–151.
[53] E.H. Hauri, Major-element variability in the Hawaiian mantle plume, Nature 382 (1996) 415–419.
[54] J.C. Lassiter, E.H. Hauri, Osmium-isotope variations in Hawaiian lavas: evidence for recycled oceanic lithosphere in the Hawaiian plume, Earth Planet. Sci. Lett. 164 (1998) 483–496.
[55] E.H. Hauri, J.A. Whitehead, S.R. Hart, Fluid dynamics and geochemical aspects of entrainment in mantle plumes, J. Geophys. Res. 99 (1994) 24275–24300.